JOURNAL OF PETROLOGY | VOLUME 47 | NUMBER 9 | PAGES 1853–1872 | 2006 | doi:10.1093/petrology/egl029

3-D Distribution of Sulphide Minerals in the Merensky Reef (Bushveld Complex, South Africa) and the J-M Reef (Stillwater Complex, USA) and their Relationship to Microstructures Using X-Ray Computed Tomography

BELINDA GODEL*, SARAH-JANE BARNES AND WOLFGANG D. MAIER

UNIVERSITÉ DU QUEBEC À CHICOUTIMI, SCIENCES DE LA TERRE, 555, BOULEVARD DE L'UNIVERSITÉ, CHICOUTIMI, QC, CANADA, G7H 2B1

RECEIVED OCTOBER 3, 2005; ACCEPTED APRIL 24, 2006; ADVANCE ACCESS PUBLICATION MAY 22, 2006

Large mafic–ultramafic layered intrusions may contain layers enriched in platinum-group elements (PGE). In many cases, the PGE are hosted by disseminated sulphides. We have investigated the distribution of the sulphides in three dimensions in two oriented samples of the Merensky Reef and the J-M Reef. The aim of the study was to test the hypothesis that the sulphides crystallized from a base metal sulphide liquid that percolated through the cumulate pile during compaction. The distribution of sulphides was quantified using: (1) X-ray computed tomography; (2) microstructural analysis of polished thin sections oriented parallel to the paleovertical; (3) measurement of dihedral angles between sulphides and silicates or oxides. In the Merensky Reef and the J-M Reef, sulphides are connected in three dimensions and fill paleovertical dilatancies formed during compaction, which facilitated the downward migration of sulphide liquid in the cumulate. In the melanorite of the Merensky Reef, the sulphide content increases from top to bottom, reaching a maximum value above the underlying chromitite layer. In the chromitite layers sulphide melt connectivity is negligible. Thus, the chromitite may have acted as a filter, preventing extensive migration of sulphide melt downwards into the footwall. This could partially explain the enrichment in PGE of the chromitite layer and the observed paucity of sulphide in the footwall.

KEY WORDS: *X-ray computed tomography; microstructures; sulphides; Merensky Reef; J-M Reef*

INTRODUCTION

Large mafic and ultramafic layered intrusions, such as the Bushveld Complex (South Africa) or the Stillwater Complex (Montana, USA) contain layers enriched in platinum-group elements (PGE) that are called 'reefs' (a mining term, which refers to a layer of rock containing mineable grades of metal). Exactly how these layers formed is still much debated, with various researchers emphasizing different processes. One school of thought suggests that the PGE crystallize directly from the magma in the form of platinum-group minerals (PGM) that accumulate on the crystal pile (Hiemstra, 1979); another suggests that the PGE were collected by a sulphide liquid that segregated from the magma and accumulated on the cumulate pile (Campbell *et al.*, 1983; Naldrett *et al.*, 1986); some workers have suggested that the PGE were collected by a fluid migrating upwards through the cumulate pile during compaction and that

*Corresponding author. Telephone: (418) 545-5011 2502. Fax: (418) 545-5012. E-mail: bgodel@uqac.ca

this fluid precipitated the sulphides and the PGE at the level of the reefs (Boudreau & McCallum, 1992; Willmore *et al.*, 2000); finally, some workers have noted that the silicates and sulphides of some reefs have undergone low-temperature alteration, which may have modified the base metal and possibly the PGE concentrations in the reef (Li *et al.*, 2004). These processes are not necessarily mutually exclusive. For example, Brenan & Rose (2002) suggested a modification of the PGM collection model, with PGM crystallizing first, followed by base metal sulphides infiltrating the crystal pile and absorbing the PGM. Barnes & Maier (2002) modified the sulphide collection model by suggesting that the PGE-rich sulphide liquid percolated through the crystal pile along dilatancies formed during compaction. To explain the extreme enrichment in IPGE (the iridium subgroup of PGE: Os, Ir and Ru) and Pt found in the Merensky Reef chromitite layers, Prichard *et al.* (2004) added a step to this model, which requires the upward migration of S-undersaturated fluid or magma. This fluid partially dissolved the accumulated base metal sulphides in the chromitite layer, creating a PGE-enriched residual sulphide. Although the exact mechanism of how PGE collection occurs remains unclear, it is clear that the PGE are found in base metal sulphides and in PGM that are associated with the sulphides (Kinloch, 1982; Ballhaus & Sylvester, 2000; Zientek *et al.*, 2002).

To better understand how the base metal sulphides and, hence, the reefs form we have investigated the distribution of sulphides in two oriented reef samples: one of the Merensky Reef at Rustenburg Platinum Mine (Bushveld Complex, South Africa); and one of the J-M Reef at Stillwater Mine (Stillwater Complex, Montana, USA). The distribution and quantity of the sulphide minerals was determined in three dimensions using X-ray computed tomography (X-ray CT). The relationship between the sulphide distribution and microstructures was investigated by examining oriented polished thin sections from these samples. In the following text, 'vertical' corresponds to the paleovertical direction.

GEOLOGICAL SETTINGS

Bushveld Complex

The Bushveld Complex (Fig. 1a) is by far the largest layered intrusion in the world (Eales & Cawthorn, 1996). The complex is 2054 ± 2·8 Ma old (Harmer & Armstrong, 2000) and has undergone very little deformation, or metamorphism, after solidification of its crystal pile. The ultramafic and mafic rocks of the Bushveld Complex are referred as the Rustenburg Layered Suite (South African Committee for Stratigraphy, 1980). The Suite is composed of five units (Fig. 1b), from bottom to top: the Marginal Zone; the Lower Zone; the Critical Zone; the Main Zone; the Upper Zone. Although there are a number of layers enriched in PGE within the intrusion, only three are sufficiently enriched in PGE, and continuous enough, to be called reefs: the Merensky Reef, the Upper Group Chromitite 2 (UG-2) and the Platreef. The Platreef is situated at the base of the intrusion, whereas the Merensky Reef and UG-2 chromitite are located in the upper part of the Critical Zone (Fig. 1b), some 2 km above the base. The sample of Merensky Reef (MR) investigated here represents normal Merensky Reef and was collected underground at Rustenburg Platinum Mines (Fig. 1a), in the southwestern portion of the Bushveld Complex. A detailed description of the Rustenburg Layered Suite at Rustenburg Platinum Mines has been given by Viljoen & Hieber (1986).

Stillwater Complex

The 2705 ± 4 Ma (Premo *et al.*, 1990) Stillwater Complex (Fig. 2a) is a layered ultramafic to mafic intrusion. Its original size is unknown as only a part of the complex is exposed along the northern margin of the Beartooth uplift of southwestern Montana (Page & Zientek, 1985). The layered rocks are divided into five series (Fig. 2b), from bottom to top: the Basal series is composed of orthopyroxene cumulates; the Ultramafic series contains various proportions of cumulus olivine, orthopyroxene and chromite; the Lower, Middle and Upper Banded series contain mainly cumulus plagioclase with minor amounts of olivine in places (McCallum *et al.*, 1980; Zientek *et al.*, 1985, 2002). As is the case in the Bushveld Complex, the Stillwater Complex contains several layers enriched in PGE, amongst them the John Manville Reef (J-M Reef) and the Picket Pin deposit. The sample studied in this work is from the J-M Reef at Stillwater Mine (Fig. 2a). The J-M Reef is associated with an olivine-bearing cumulate (OB-1) of the Lower Banded series (Barnes & Naldrett, 1985; Turner *et al.*, 1985; Zientek *et al.*, 1985, 2002). Unlike the Bushveld Complex, the Stillwater Complex has undergone regional deformation and metamorphism (Zientek *et al.*, 2002).

METHODS

X-ray computed tomography

Principles and methods

X-ray computed tomography (X-ray CT) is an entirely non-destructive technique that allows visualization and reconstruction of the internal structure of solid objects in three dimensions. Initially, X-ray CT was developed and used as a medical imaging technique (Hounsfield, 1973). However, this technique can also be used for qualitative and quantitative analysis of geological materials (Ketcham *et al.*, 2001) such as metamorphic rocks

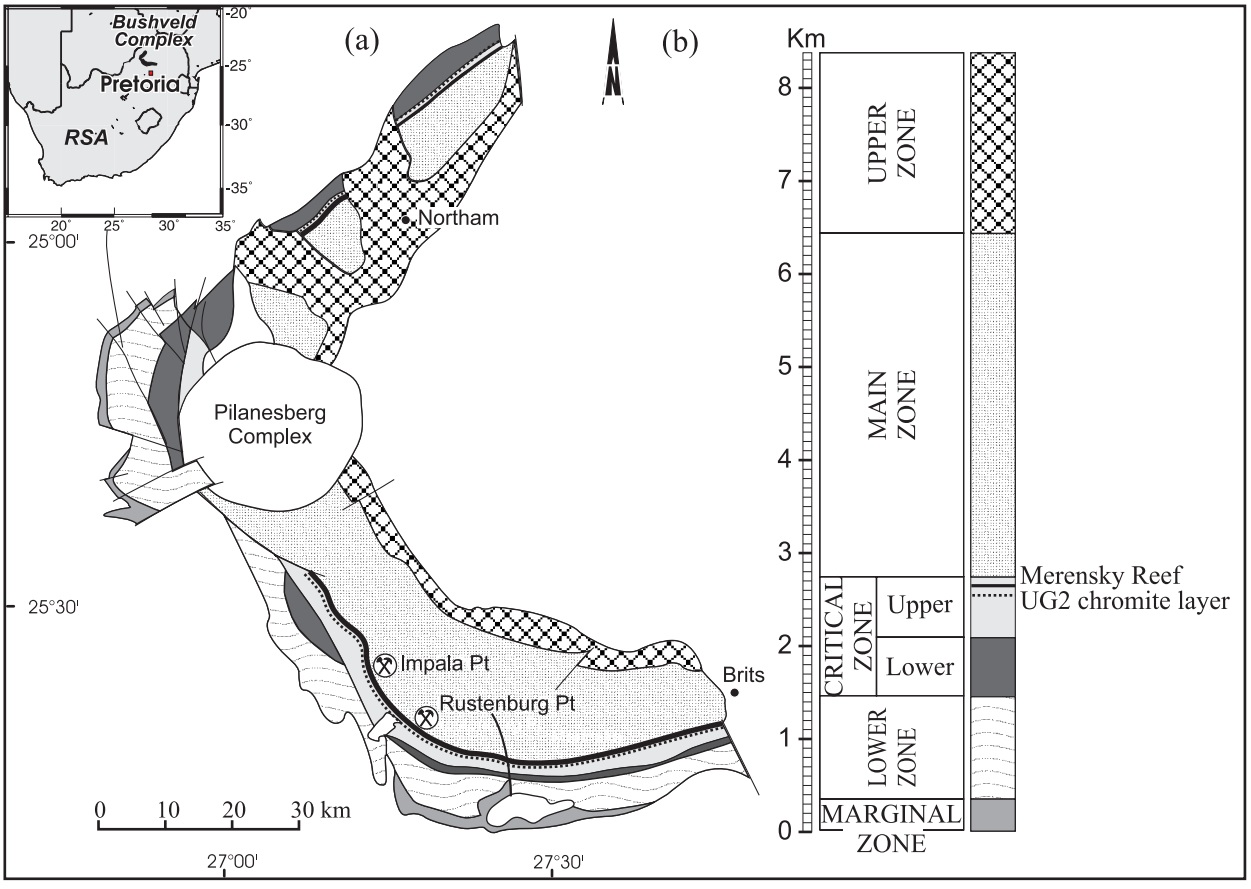

Fig. 1. Details of the geology of the western lobe of the Bushveld Complex, Republic of South Africa (RSA). (a) Simplified geological map of the western lobe of the Bushveld Complex (modified after Von Gruenewaldt, 1986, 1989). (b) Generalized stratigraphy of the Bushveld Complex (modified after Eales & Cawthorn, 1996).

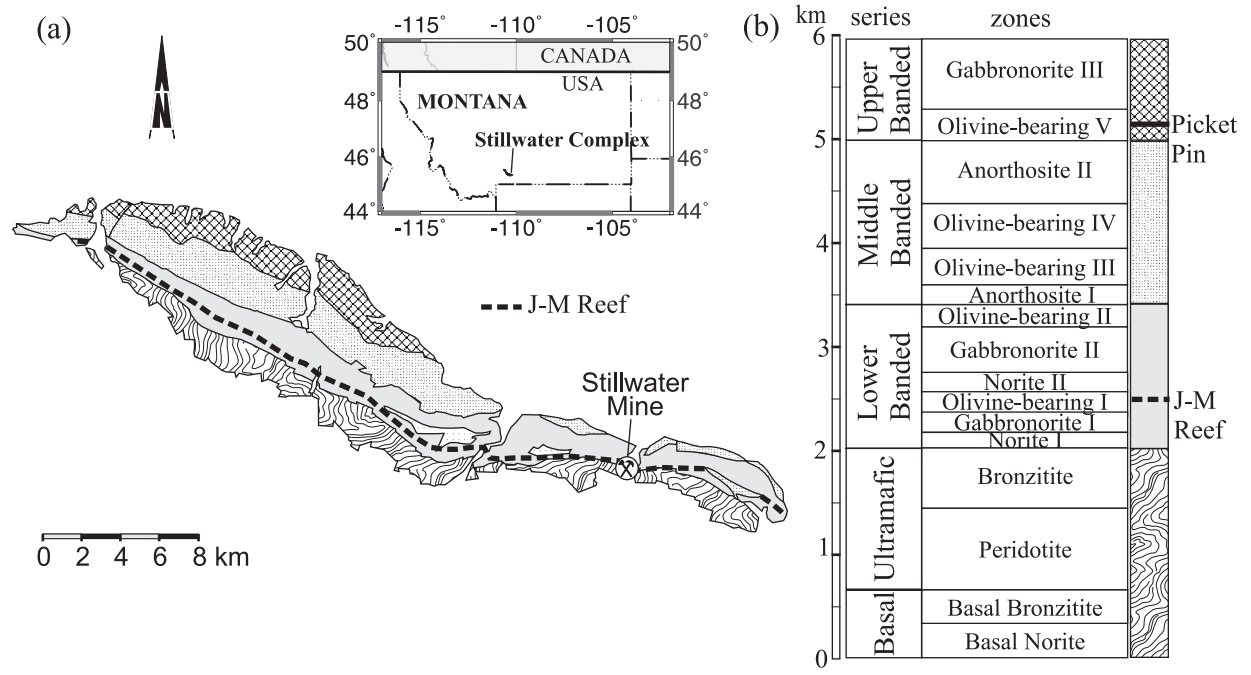

Fig. 2. Details of the geology of the Stillwater Complex, Montana, USA. (a) Simplified geological map of the Stillwater Complex (modified after McCallum *et al.*, 1980; Zientek *et al.*, 2002). (b) Generalized stratigraphy of the Stillwater Complex (modified after Zientek *et al.*, 2002).

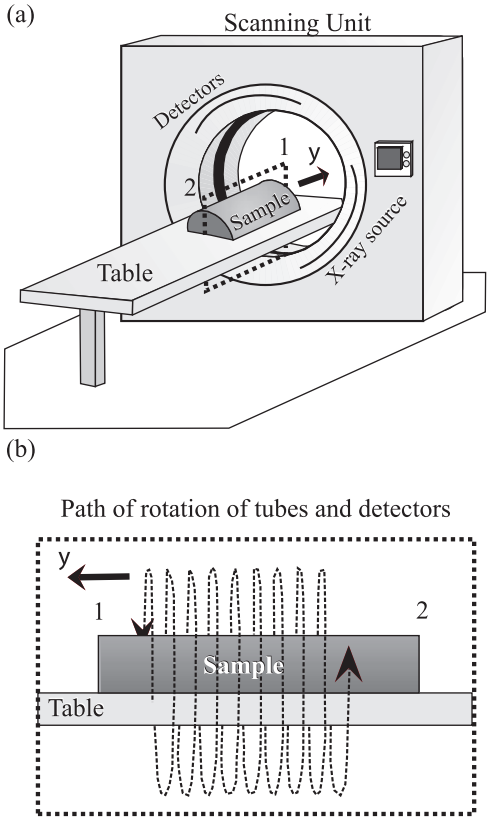

Fig. 3. Schematic diagram of the X-ray computed tomography (CT) scanner. (a) The CT system comprises principally a scanning unit composed of detectors and X-ray sources (tubes), and a table on which the samples were positioned to undergo scanning. (b) The sample on the table is moved through the scanner in the *y*-direction while the gantry performs multiple 360° rotations around the sample. Consequently, X-rays trace a spiral around the sample and produce a data volume created by a multitude of 3-D pixels called 'voxels'. Images ('slices') are generated using special reconstruction principles and filtering techniques. The 3-D view is obtained by stacking all the slices.

(Carlson & Denison, 1992; Denison & Carlson, 1997; Denison *et al.* 1997), sedimentary rocks (Flisch & Becker, 2003; Michaud *et al.*, 2003), soils (Delerue *et al.*, 2003), meteorites (Kondo *et al.*, 1997), fossils (Brochu, 2000) or ores (Kyle & Ketcham, 2003; Kyle *et al.*, 2004). The details of the principle and the functioning of X-ray CT have been developed in many papers (Denison *et al.*, 1997; Ketcham & Carlson, 2001; Mees *et al.*, 2003; Ketcham & Iturrino, 2005) and only a brief description is given here.

In this study, the samples were scanned at the INRS (Institut Nationale de la Recherche Scientifique, Quebec, Canada) using an X-ray CT scanner 'Siemens Somatom Volume Access'. The CT system is described in Fig. 3. An important aspect of this scanner is that samples with a length of several tens of centimetres can be scanned. The scanning unit (more precisely, the tubes) can be operated at maximum power for a limited time only. This reduces its capacity to scan a large sample at high resolution. Consequently, because of the size of the Merensky Reef sample, and to obtain a better resolution, data for this sample were collected in two continuous steps (the second scan starting at the position of the last slice of the first scan incremented by one slice thickness).

The X-ray tubes were operated at 140 kV accelerating potential and 112 mA current for the J-M Reef and at 140 kV accelerating potential and 245 mA current for the Merensky Reef. The images were reconstructed using a filtered back-projection and corrections to reduce the effect of beam-hardening or ring artefact (see further description) at INRS. The output images were then digitized as DICOM (Digital Imaging and Communication in Medicine) formatted 16-bit files with 512 × 512 pixels. Merensky Reef voxels (i.e. pixels in three dimensions) are 0·25 mm × 0·25 mm × 1 mm, and J-M Reef voxels are 0·125 mm × 0·125 mm × 0·5 mm, where the larger dimension is the vertical one. In this study, 305 slices were obtained for the Merensky Reef and 219 slices were obtained for the J-M Reef. Each slice is a map of the variation of X-ray attenuation across the sample. X-rays are attenuated through the sample of rock following the Beer–Lambert Law (Boespflug *et al.*, 1995):

$$I = I^{\circ} e^{-\mu h}$$

where I° is the initial intensity of the incident X-ray beam, I is the intensity measured by the detector, h is the sample thickness and μ is a linear attenuation coefficient, which depends on the average atomic number and the density of the material. The attenuation coefficient of the sample (μs) is expressed in tomographic intensity (TI), or in CT number (CT) (Hounsfield, 1973):

$$TI = (\mu s/\mu w - 1) \times 1000$$

where μw is the attenuation coefficient of water. Using the CT scanner settings, the variation of X-ray attenuation shows the distribution of specific minerals across the sample.

All further image processing, analysis and stacking for the determination and quantification of sulphide mineral distribution were performed using 3D-Doctor (Able Software Corp.), IDL (Interactive Data Language, Research Systems Inc.) and GMT (Wessel & Smith, 1998) software.

Definition of sulphide mineral boundaries

For each slice, the sulphide mineral boundaries were defined using a segmentation (threshold) value. In our case, the sulphide minerals are intergrowths of pyrrhotite, pentlandite and chalcopyrite (the proportions of each

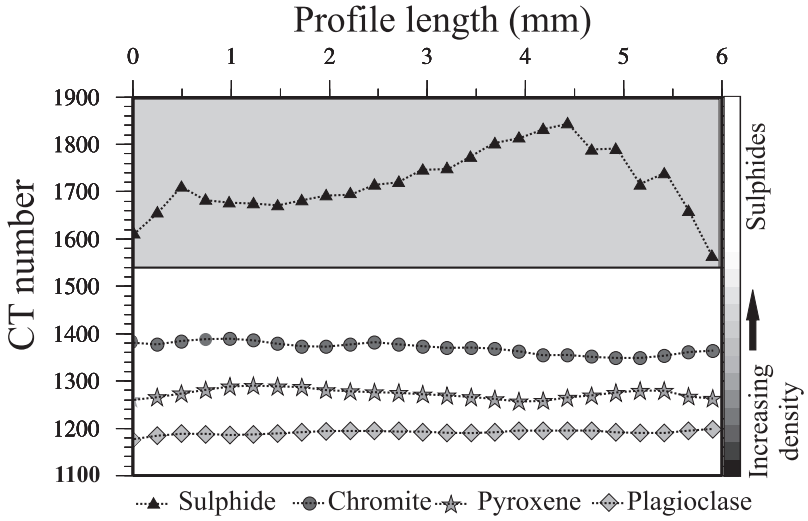

Fig. 4. Profiles of CT number across minerals, calculated using the slices obtained by the CT scan. Minerals observed in thin sections are compared with the corresponding minerals observed on the slices. The profile length corresponds to the length or width of a specific mineral. Sulphide minerals are characterized by a CT number >1540 (see text for explanation).

phase vary as a function of the lithology, but on average they are ~40% pyrrhotite, ~40% pentlandite and 20% chalcopyrite). These sulphides also contain significant amounts (up to 800 ppm) of PGE in solid solution (Ballhaus & Ryan, 1995; Ballhaus & Sylvester, 2000).

To access the sulphide distribution in both samples correctly, CT scan results were compared with the corresponding thin sections (i.e. the same minerals). Profiles of CT number were determined across known (i.e. observed both on slices and corresponding thin sections) sulphides and others minerals of various sizes. Examples of profiles obtained for the different minerals are given in Fig. 4. All results for sulphides were then compared and an optimal segmentation value for our sulphides was defined using the minimum CT number obtained for the sulphides as the lower boundary. This threshold value is 1540; all minerals with a CT number >1540 are sulphides. Consequently, the volume of sulphides in our sample was calculated by summing all voxels with a CT number >1540 (see further description).

Artefacts and uncertainty on measurements

X-ray CT sometimes produces images in which some peculiar features are artefacts (caused by beam-hardening, ring artefacts or partial-volume effects for example). The characteristics of these artefacts have been reviewed in detail in the literature (Denison *et al.*, 1997; Ketcham & Carlson, 2001; Mees *et al.*, 2003) and no further description is presented here. Beam-hardening and ring artefacts were minimized by using a correction and filter during the reconstruction and the post-processing at INRS. The sulphide minerals and silicates (essentially pyroxene and plagioclase) considered in this work have very different attenuation values and the sulphides are randomly oriented. Following Wellington & Vinegar (1987) and Johns *et al.* (1993), the errors caused by partial-volume effects can be neglected without significant consequences for the measurements.

To estimate the uncertainties on the measurements of the sulphide volume, the final results obtained by CT scan were compared with the macroscopic and microscopic observations (Fig. 5). The CT image of the sulphides (the inset in Fig. 5b) was compared with the corresponding image in thin section (Fig. 5c). First, the number of pixels with CT number >1540 (i.e. corresponding to the sulphide) was calculated, then this result was compared with the area enclosed by the sulphide in the thin section. The uncertainty on the measurement was calculated by comparing the number of pixels obtained in both cases. This uncertainty on the measurement of the sulphide volume by the CT scan is ~5%. Another uncertainty on the sulphide volume calculation arises from the presence of small sulphides (i.e. having a size lower than the voxel size; see below) that were not included in the calculation. The sulphides observed in the thin sections of all lithologies (except the anorthosite) are larger than than the voxel size (in ~90% of cases). In the anorthosite, a few sulphides (~0·1%) were observed in thin section but were usually not identified and measured by the CT scan analysis. As these sulphides in the anorthosite are very small and rare, they have no real effect on the sulphide volume calculation. However, to take into account the small (less than voxel size) sulphides, the uncertainty on the measurement was overestimated to 10% (Tables 1 and 2).

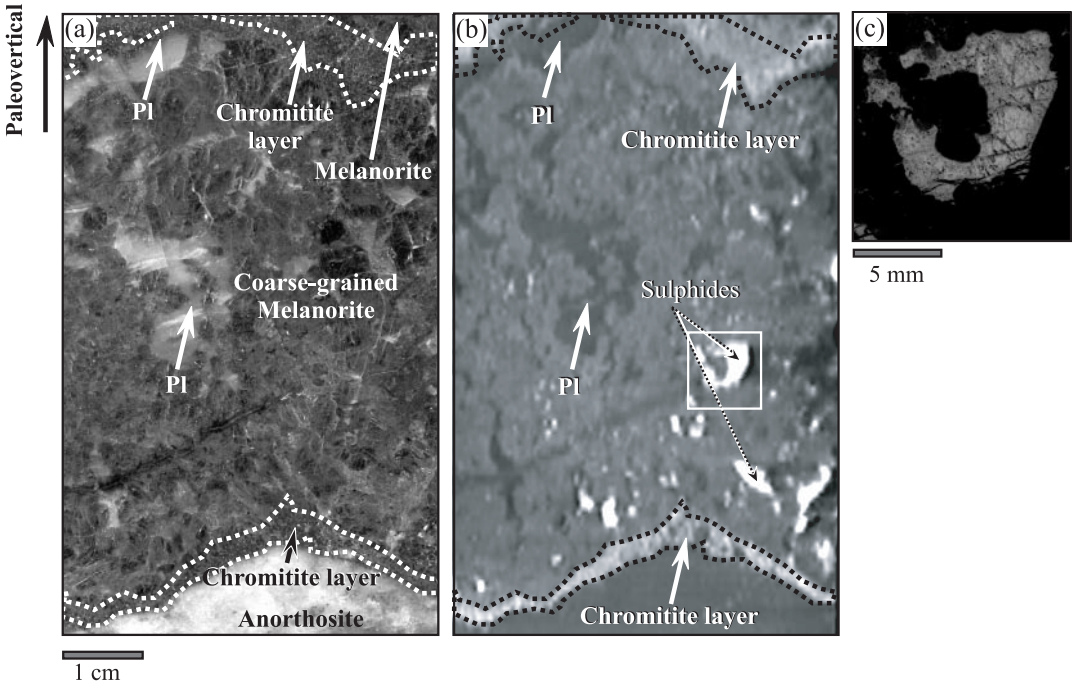

Fig. 5. Comparison between results obtained by CT scan and by macroscopic and microscopic observations for the Merensky Reef sample. (a) Photograph of a part of the polished slab of the Merensky Reef sample. (b) Slice obtained by CT scan corresponding to photograph (a). The images are displayed in greyscale, where dark grey and white correspond to materials of lower and higher density, respectively. (c) Part of a thin section showing sulphides (in reflected light), which corresponds to the inset in (b). From bottom to top, the sample shown is made up of: a layer of anorthosite; a layer of chromitite (lower chromitite) containing sulphides [white in (b)]; a coarse-grained melanorite [grey in (b)] with interstitial plagioclase [dark grey in (b)] and containing sulphides that are visible only on the slice analysed by CT scan (b); a second layer of chromitite (upper chromitite). Sulphides observed in (b) show a good shape correlation with the same sulphides observed in thin section (c).

Analysis of microstructures

To determine whether there is a relationship between sulphide distribution and microstructures in the two samples, oriented polished thin sections were examined with an optical microscope. For the MR sample, thin sections were oriented so that the long axis corresponds to the paleovertical. For the J-M Reef sample, the paleovertical was represented by the short axis (the long axis corresponding to the width of the drill-core). The presence and orientation of the optical microstructures were then compared with the three-dimentional (3-D) distribution of the sulphides obtained by X-ray CT. Finally, to characterize sulphide melt connectivity in the MR sample, measurements from the thin sections were used for the calculation of dihedral angles.

PETROGRAPHY

Merensky Reef sample

The MR sample is an oriented polished slab of 30 cm height, 11 cm width and on average 3·5 cm thickness. Our sample resembles other MR samples described by a number of researchers. It consists, from the bottom to the top, of a layer of anorthosite overlain by a chromitite layer of variable thickness (between 2 and 7 mm), ~11 cm of coarse-grained melanorite (which some workers refer to as a 'pegmatoidal pyroxenite'), a second chromitite of variable thickness (between 3 and 10 mm), and finally melanorite. The sample contains between 0·5 and 6 vol. % sulphide minerals, disseminated throughout the various layers in the sample, with the exception of the basal anorthosite, which contains very little sulphide. In all rock types the sulphide phases are made up of intergrowths of pyrrhotite, pentlandite, and chalcopyrite.

The layer of anorthosite is composed of ~95 modal % cumulus plagioclase and ~5% oikocrysts of orthopyroxene with minor (<0·5%) randomly distributed sulphide minerals. The plagioclase grains are subhedral with a grain size ranging from ~1 to ~5 mm. The long axes of the larger plagioclase grains are oriented parallel to the horizontal direction and parallel to the contact with the overlying chromitite. These plagioclase crystals have rectilinear twins (i.e. igneous twins) and few of them are zoned. The anorthosite is not deformed and the preferred orientation of the plagioclase is interpreted as an igneous lamination.

The contact between the anorthosite and the overlying chromitite undulates on a centimetre scale (Fig. 5a). The chromitite is made up of ~50% amoeboidal to

Table 1: Calculated sulphide mineral content and lithologies in the Merensky Reef sample

Height* (mm)	Lithology† (%)					Vol. % sulphide	Host of sulphide‡ (%)				
	M	UC	CGM	LC	An		M	UC	CGM	LC	An
270	100	—	—	—	—	<0·1	0	0	0	0	0
265	100	—	—	—	—	<0·1	0	0	0	0	0
260	100	—	—	—	—	<0·1	0	0	0	0	0
255	100	—	—	—	—	0·1 ± <0·1	100	0	0	0	0
250	100	—	—	—	—	0·3 ± <0·1	100	0	0	0	0
245	100	—	—	—	—	1·0 ± 0·1	100	0	0	0	0
240	100	—	—	—	—	0·9 ± 0·1	100	0	0	0	0
235	100	—	—	—	—	0·1 ± <0·1	100	0	0	0	0
230	100	—	—	—	—	0·2 ± <0·1	100	0	0	0	0
225	100	—	—	—	—	0·7 ± 0·1	100	0	0	0	0
220	100	—	—	—	—	1·5 ± 0·2	100	0	0	0	0
215	100	—	—	—	—	1·1 ± 0·1	100	0	0	0	0
210	100	—	—	—	—	0·5 ± <0·1	100	0	0	0	0
205	100	—	—	—	—	0·2 ± <0·1	100	0	0	0	0
200	100	—	—	—	—	0·1 ± <0·1	100	0	0	0	0
195	100	—	—	—	—	0·2 ± <0·1	100	0	0	0	0
190	100	—	—	—	—	0·4 ± <0·1	100	0	0	0	0
185	100	—	—	—	—	1·0 ± 0·1	100	0	0	0	0
180	100	—	—	—	—	0·1 ± <0·1	100	0	0	0	0
175	100	—	—	—	—	<0·1	100	0	0	0	0
170	100	—	—	—	—	<0·1	100	0	0	0	0
165	100	—	—	—	—	<0·1	100	0	0	0	0
160	100	—	—	—	—	<0·1	100	0	0	0	0
155	100	—	—	—	—	0·2 ± <0·1	100	0	0	0	0
150	100	—	—	—	—	1·2 ± 0·1	100	0	0	0	0
145	100	—	—	—	—	3·7 ± 0·4	100	0	0	0	0
140	100	—	—	—	—	5·9 ± 0·6	100	0	0	0	0
135	100	—	—	—	—	4·2 ± 0·4	100	0	0	0	0
130	100	—	—	—	—	3·0 ± 0·3	100	0	0	0	0
125	100	—	—	—	—	3·7 ± 0·4	100	0	0	0	0
120	100	—	—	—	—	2·7 ± 0·3	100	0	0	0	0
115	53	34	13	—	—	2·2 ± 0·2	95	5	0	0	0
110	40	27	31	—	—	2·4 ± 0·2	40	60	0	0	0
105	30	24	46	—	—	2·2 ± 0·2	54	41	5	0	0
100	16	18	66	—	—	1·1 ± 0·1	65	26	9	0	0
95	—	6	94	—	—	1·0 ± 0·1	43	39	18	0	0
90	—	—	100	—	—	<0·1	0	0	100	0	0
85	—	—	100	—	—	<0·1	0	0	100	0	0
80	—	—	100	—	—	0·1 ± <0·1	0	0	100	0	0
75	—	—	100	—	—	0·2 ± <0·1	0	0	100	0	0
70	—	—	100	—	—	0·3 ± <0·1	0	0	100	0	0
65	—	—	100	—	—	1·2 ± 0·1	0	0	100	0	0
60	—	—	100	—	—	<0·1	0	0	100	0	0
55	—	—	100	—	—	0·5 ± <0·1	0	0	100	0	0
50	—	—	100	—	—	2·1 ± 0·2	0	0	100	0	0
45	—	—	100	—	—	3·8 ± 0·4	0	0	100	0	0

Table 1: continued

Height* (mm) sulphide	Host of					Lithology† (%) sulphide‡ (%)	Vol. %				
	M	UC	CGM	LC	An		M	UC	CGM	LC	An
40	—	—	100	—	—	1·1 ± 0·1	0	0	100	0	0
35	—	—	100	—	—	2·0 ± 0·2	0	0	100	0	0
30	—	—	100	—	—	3·3 ± 0·3	0	0	100	0	0
25	—	—	100	—	—	2·2 ± 0·2	0	0	100	0	0
20	—	—	100	—	—	2·9 ± 0·3	0	0	100	0	0
15	—	—	95	5	—	5·5 ± 0·5	0	0	99	1	0
10	—	—	70	27	9	1·9 ± 0·2	0	0	98	2	0
5	—	—	30	30	40	0·8 ± <0·1	0	0	57	43	0
0	—	—	4	15	83	1·1 ± 0·1	0	0	12	88	0
−5	—	—	—	—	100	<0·1	0	0	0	0	100
−10	—	—	—	—	100	<0·1	0	0	0	0	100
−15	—	—	—	—	100	<0·1	0	0	0	0	100
−20	—	—	—	—	100	<0·1	0	0	0	0	100
−25	—	—	—	—	100	<0·1	0	0	0	0	100

*Height above the base of the Lower Chromitite layer.
†Average lithology calculated from CT scan slices.
‡Lithology (calculated from CT scan slices) of host of the total sulphide minerals. M, melanorite; UC, upper chromitite; CGM, coarse-grained melanorite; LC, lower chromitite; An, anorthosite.

euhedral chromite, ~40% poikilitic plagioclase, ~9% orthopyroxene, and ~1% sulphide minerals. The silicate minerals show signs of high-temperature deformation. Oikocrysts of plagioclase show deformation twins (Fig. 6). Furthermore, plagioclase and orthopyroxene exhibit undulose extinction. Three different forms of sulphides are present as: (1) inclusions in chromite grains; (2) disseminated grains at the contacts between chromite and plagioclase, or pyroxene, grains; (3) inclusions in unstrained poikilitic plagioclase or pyroxene.

The contact between the lower chromitite and the overlying melanorite also undulates on a centimetre scale (Fig. 5). The melanorite is made up of ~70% coarse-grained orthopyroxene crystals (ranging from 2 to 10 mm in width), ~20% interstitial plagioclase, ~7% euhedral chromite grains, ~1% biotite, and ~2% interstitial sulphide minerals. As described by Barnes & Maier (2002), large orthopyroxenes seem to be the product of suturing of several smaller orthopyroxene grains, and the contacts between original small orthopyroxene grains are marked by trains of small euhedral chromite grains. Furthermore, in one thin section, interstitial sulphide minerals are present along the sutures between the original, smaller orthopyroxene grains. Orthopyroxene grains are indented and exhibit undulose extinctions. Some orthopyroxenes have clinopyroxene exsolution blebs (Fig. 6c) oriented parallel to cleavage planes. Plagioclase exhibits both deformation twins and rectilinear twins (Fig. 6a, b and f).

The contact between the melanorite and the upper chromitite is irregular. The chromitite layer is made up of ~50% cubic chromite grains, ~25% poikilitic unstrained plagioclase crystals, ~24% orthopyroxene oikocrysts, and ~1% sulphide minerals. Some of the chromite grains occur along orthopyroxene sutures (Fig. 6a). Oikocrysts of plagioclase and orthopyroxene both exhibit undulose extinction. Furthermore, plagioclase shows extensive development of deformation twins (see further description in caption to Fig. 6).

The melanorite at the top of the sequence (Fig. 6f) is made up of ~60% subhedral orthopyroxene, ~20% interstitial and poikilitic plagioclase, ~10% clinopyroxene, ~6% chromite, ~2% biotite and ~2% sulphide minerals. In some cases, plagioclase exhibits kink bands and deformation twins (Fig. 6e). Many of the orthopyroxene crystals are indented and show undulose extinction and kinking (Fig. 6b and f). In a few cases, cleavage planes in orthopyroxene are curved around the indentations, suggesting that bending of the lattice has occurred. Sulphide minerals are located along orthopyroxene grain boundaries, which in some cases impinge on each other, or are kinked.

Table 2: Sulphide mineral content in the J-M Reef

Depth (mm)	Sulphide (vol. %)	Depth (mm)	Sulphide (vol. %)
2·5	2·3 ± 0·2	52·5	6·2 ± 0·6
7·5	6·6 ± 0·7	57·5	8·9 ± 0·9
12·5	4·6 ± 0·5	62·5	9·1 ± 0·9
17·5	4·6 ± 0·5	67·5	5·4 ± 0·5
22·5	9·6 ± 1·0	72·5	8·0 ± 0·8
27·5	13·1 ± 1·3	77·5	10·5 ± 1·0
32·5	8·2 ± 0·8	82·5	7·7 ± 0·8
37·5	7·5 ± 0·8	87·5	8·2 ± 0·8
42·5	12·4 ± 1·2	92·5	6·1 ± 0·6
47·5	8·9 ± 0·9	97·5	3·0 ± 0·3

J-M Reef sample

The J-M Reef sample was collected from a drill-core at the Stillwater Mine oriented along the paleovertical. The sample consists of olivine melagabbronorite and is 11 cm height, an average of 5 cm wide and an average of 1·5 cm thick. It contains ~62% pyroxene, ~15% olivine, ~15% plagioclase, ~3% biotite and an average of ~5% disseminated sulphides composed of pyrrhotite, pentlandite and chalcopyrite. Some of the orthopyroxene crystals contain inclusions of clinopyroxene along cleavage planes. Sulphides generally define a vertical network between deformed pyroxenes and rounded olivine crystals (Fig. 7). Secondary chalcopyrite is recrystallized in tremolite + actinolite + calcite alteration zones around silicate minerals such as olivine or pyroxene (Fig. 7). The chalcopyrite is oriented perpendicular to the crystal faces of the silicate phases. This alteration occurs only at contacts between silicate minerals and sulphides. As previously described for the UG-2 and the Merensky Reef by Li *et al.* (2004), the alteration could be due to the interaction between the base metal sulphides and a low-temperature aqueous fluid. Furthermore, in some parts of the thin sections, myrmekitic textures were observed. These structures have previously been described by McCallum *et al.* (1980) and according to the mine geologists are found in many samples (E. Geraghty, personal communication, 2005).

RESULTS

3-D distribution of sulphide minerals

Stacking the slices (obtained by CT scan) shows the 3-D distribution of sulphide minerals (3-D animations of both samples are available online at http://petrology.oxfordjournals.org/) within the sample (Figs 8b and 9a) or a sub-volume. To quantitatively measure the sulphide mineral distribution across each sample, the position and volume of the sulphide minerals were calculated (Figs 8c and 9b).

Calculation methods for quantitative analysis of the distribution of sulphide minerals

To quantify the distribution of sulphide, a sub-volume entirely enclosed by the Merensky Reef sample was defined. The new, virtual, parallelepiped sample volume is 282 mm high, 67 mm wide and 12·75 mm thick (Fig. 8b). The J-M sample is a part of a drill core, and thus its shape is relatively constant. Consequently, contrary to the MR sample, the entire sample was taken into account. Sulphide grain boundaries were defined in each lithology using the minimum threshold CT value of 1540 (as described above). Sulphide volume was then calculated by summing the voxels with a CT number >1540. Results were smoothed by averaging the data for five slices (for MR) and 10 slices (for the J-M Reef), representing 5 mm in height according to the paleovertical (Figs 8c and 9b, Tables 1 and 2).

3-D distribution of sulphides in the Merensky Reef sample

Variation of the sulphide mineral content as a function of paleovertical position (zero being arbitrarily defined as the base of the lower chromitite and height increases up-section) shows that the sulphides are present in chromitite layers and melanorites, but are rare in the anorthosite (Fig. 8b and c, and Tables 1 and 2). The presence of ~0·1 to 5·9 ± 0·6% sulphides in the chromitite and melanorite is confirmed by petrographic observation.

The amount of sulphides present in the lower chromitite layer is 0·9 ± 0·1% (Table 1 and Fig. 8c). This increases up-section into the coarse-grained melanorite to reach a maximum of 5·5 ± 0·5% at a height of 15 mm above the lower chromitite (Fig. 8c). Thereafter the amount of sulphide decreases up-section to <0·1% at a height of 90 mm. In the upper chromitite layer the sulphide content increases from 1·0 ± 0·1% (at 95 mm) to 2·2 ± 0·2% (at 115 mm) and continues to increase in the overlying melanorite to reach a maximum of 5·9 ± 0·6% at 140 mm above the lower chromitite seam. In the remainder of the melanorite, the sulphide content is generally low (~0·2%), but there are three peaks at 185 mm, 220 mm and 240 mm where the sulphide content rises above 1·0 ± 0·1%.

In the melanorites, sulphide minerals are distributed along networks that are oriented sub-parallel to the paleovertical (Fig. 8b) and that are 10–40 mm in height. These networks terminate in the underlying chromitite,

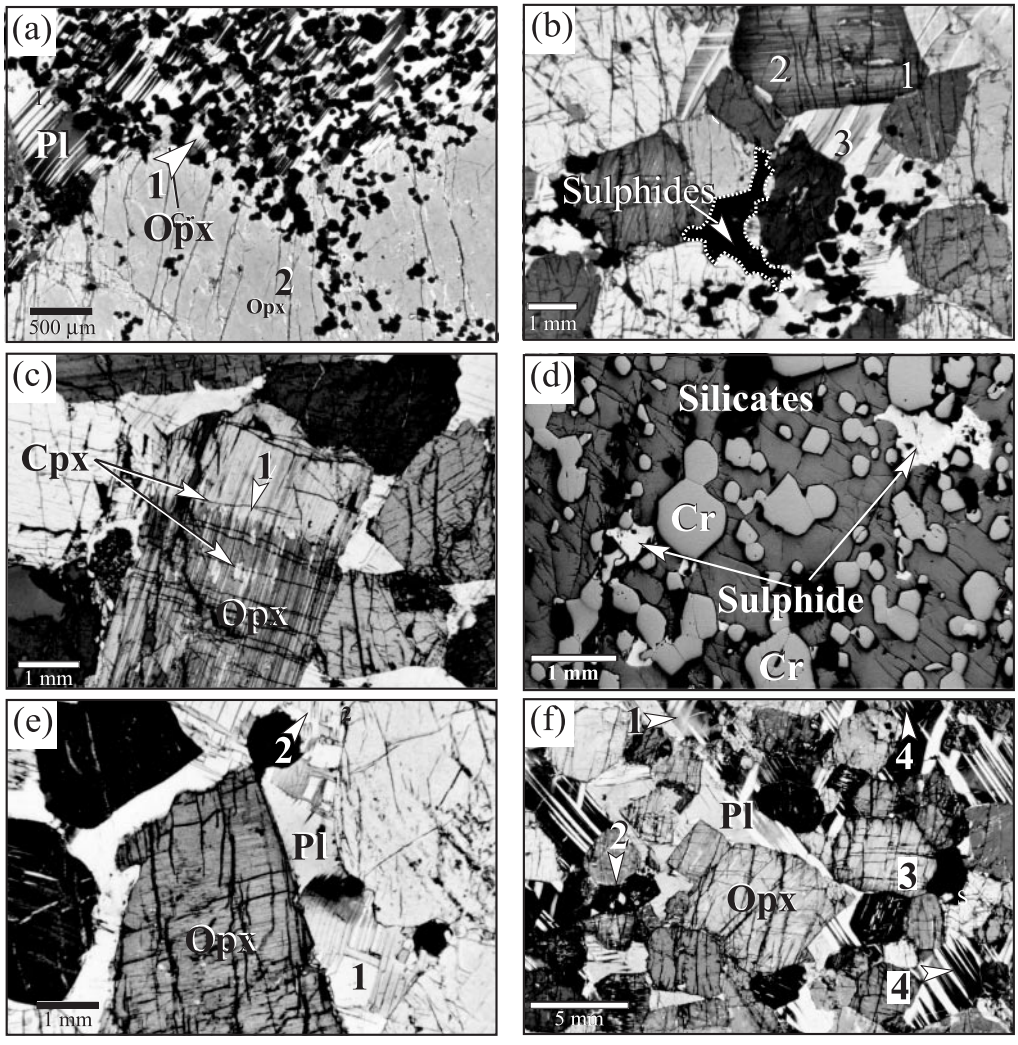

Fig. 6. Photomicrographs of microstructures observed in the Merensky Reef sample. All photomicrographs are oriented with the paleovertical upwards. Opx, orthopyroxene; Pl, plagioclase; Cpx, clinopyroxene; Cr, chromite; S, sulphide minerals; Px, pyroxene. (a) Contact between upper chromitite and the underlying melanorite. Pl enclosing Cr grains exhibit extensive deformation twins (1) oriented close to the paleovertical. Cr grains along contact between Opx grains (2) should be noted. (b) Melanorite with interstitial sulphides located along Opx crystal faces. Some Opx have indented contacts (1) and subgrains (2) developed between Opx contacts. Furthermore, Pl have bent twins (3) and undulose extinction. (c) Kink band (1) in Opx crystal and exsolution of Cpx along Opx cleavages as a result of strain on Opx lattice. (d) Sulphides in chromitite layer (in reflected light). (e) Deformation band (1) and deformed twins (2) in interstitial Pl in melanorite. (f) Melanorite with interstitial sulphide and deformation features in Px and Pl: (1) undulose extinctions in Pl; (2) indented contacts in Px; (3) undulose extinctions in Px; (4) spindle-shaped twins in Pl.

and the sulphides are generally more abundant above troughs in the chromitite layers (Fig. 8b).

By considering the qualitative and quantitative 3-D distribution of sulphide minerals, several features can be highlighted: (1) there is a peak in sulphide content a few centimetres above the chromitite layers, after which the sulphide content in both melanorites decreases up-section; (2) the distribution of sulphide minerals correlates with variations in the shape of the chromitite layer in that sulphides are more abundant above troughs in the chromitite; (3) there are very few sulphide minerals in the anorthosite.

J-M Reef sample

In thin sections, sulphide minerals form connected vertical networks along the grain boundaries of silicate grains (Fig. 7). This feature was also observed in the 3-D scans (Fig. 9a). The areas of sulphide minerals have various sizes from 1 mm to 2 cm, but they have a relatively constant elongate shape. The quantitative analysis (Fig. 9b and Table 2) indicates that, overall, sulphide minerals represent about $7{\cdot}6 \pm 0{\cdot}76$ vol. % of the rock. The sulphide content ranges from $2{\cdot}3 \pm 0{\cdot}2$ to $13{\cdot}1 \pm 1{\cdot}3$ vol. % and does not appear to show any correlation with height in the core sample. At the bottom right of

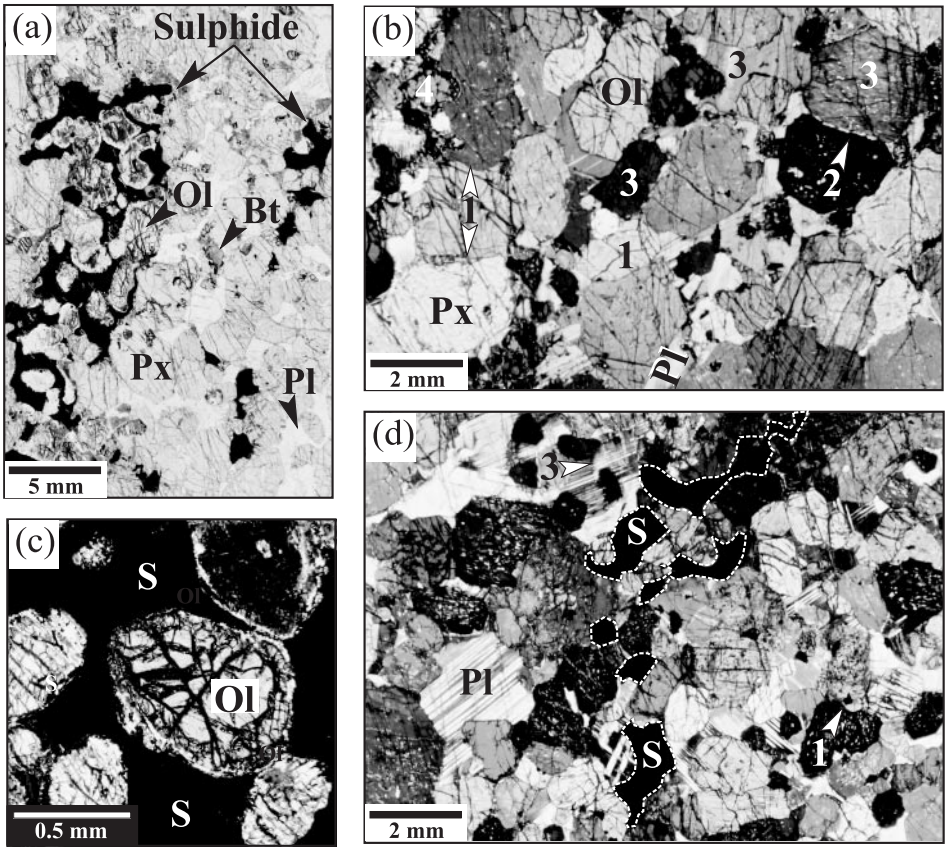

Fig. 7. Photomicrographs of microstructures observed in the J-M Reef sample. All photomicrographs are oriented with paleovertical upwards. S, sulphide minerals; Px, pyroxene; Pl, plagioclase; Ol, olivine; Bt, biotite. (a) Olivine melagabbronorite with interstitial sulphides (black) located in vertical networks along silicate grain boundaries. (b) Olivine melagabbronorite with deformation features and sulphides located along vertical network. Deformation is marked by: (1) indented contacts to Px; (2) development of subgrains at Px contacts; (3) undulose extinction in both Px and Pl; (c) rounded olivines surrounded by sulphide minerals. The corona formed by a mixture of alteration mineral and chalcopyrite around olivine grains should be noted. (d) Deformed olivine melagabbronite with interstitial sulphide minerals located along a vertical network. Numbers are the same as in (b).

the sample, massive sulphides are present and occupy a volume of about 2 cm width, 0·5 cm height and 0·5 cm thickness. The thin-section information (Fig. 7d) is interpreted as evidence that sulphide liquids have percolated downward through the pyroxene and olivine framework and have been collected, or trapped, in this small volume.

Microstructural analysis

Deformation during crystallization

Merensky Reef sample. Both samples (MR and J-M Reef) exhibit high-temperature crystal deformation features. Microstructures observed in this study are very similar to those observed by Barnes & Maier (2002) in samples from the Merensky Reef at Impala Platinum mines. In the chromitite layers and the melanorites, the orthopyroxene, clinopyroxene, and plagioclase all exhibit high-temperature deformation features. In both melanorite layers, several cumulus orthopyroxene crystals impinge on each other and have produced indented contacts (Fig. 10a). The indented contacts are close to the horizontal direction, whereas the vertical contacts are not indented. In many cases, cleavage planes and exsolution lamellae are straight near the contacts between minerals, indicating that, in most cases, diffusion creep or dissolution has occurred. However, in one case (Fig. 10), the cleavage planes are curved around the indentation, indicating that bending of the lattice has also occurred. In both the melanorites and the upper chromitite layer, orthopyroxene shows undulose extinction and contains deformation bands (Fig. 10). Furthermore, small subgrains are developed at the horizontal contacts between some of the pyroxene crystals (Fig. 10). This indicates that part of the deformation in the pyroxene was by dislocation creep.

The interstitial plagioclase shows undulose extinction, many deformation twins (spindle-shaped perpendicular and bent twins), and deformation bands (Fig. 10). The

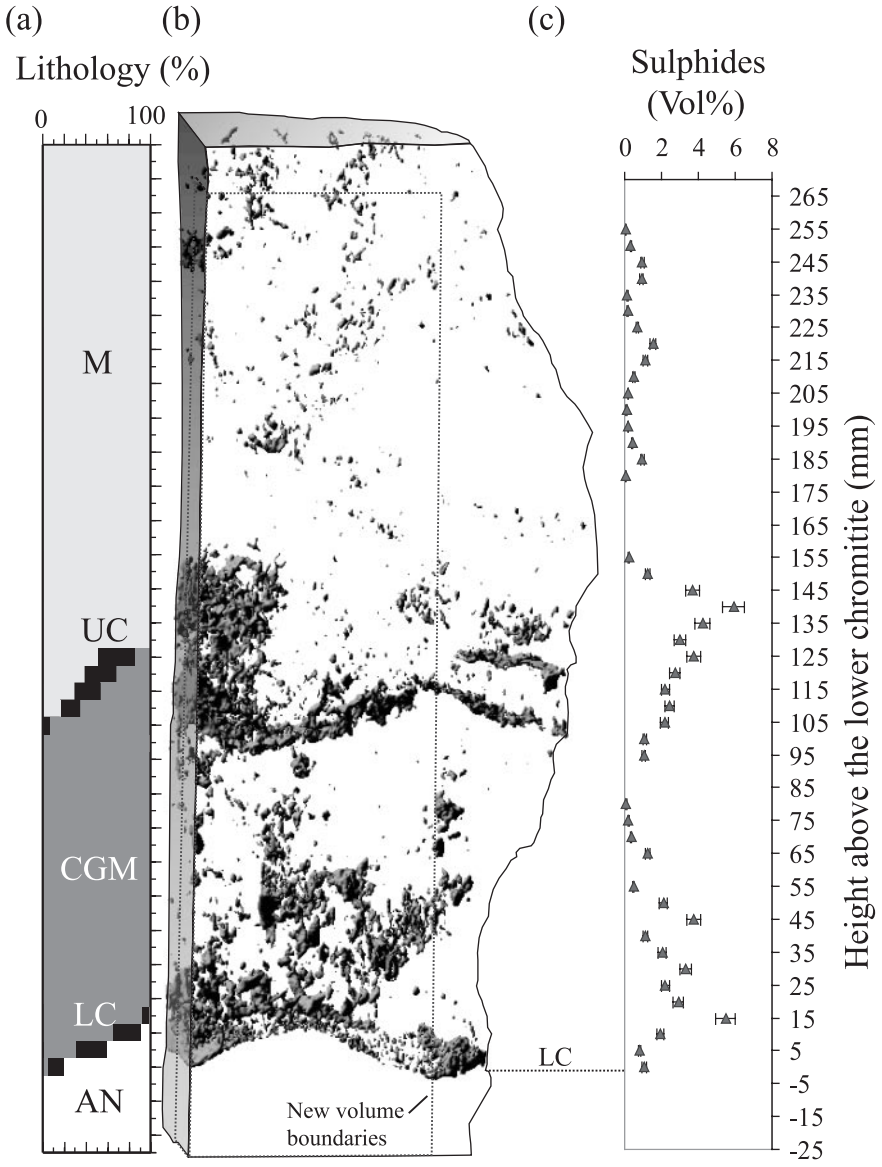

Fig. 8. Distribution of sulphide minerals in the Merensky Reef sample based on results from CT scans. All calculations have been made using a new defined volume [dotted line in (b)] entirely enclosed by the sample. (a) Lithology calculated from CT scan slices. (b) 3-D visualization with sulphides represented by black and grey shading. (c) Quantification of sulphide mineral content (see text for calculation method). Zero is arbitrarily defined as the base of the lower chromitite and height increases up-section. M, melanorite; UC, upper chromitite; CGM, coarse-grained melanorite; LC, lower chromitite; AN, anorthosite.

deformation twins have a preferred shape orientation (Fig. 10) close to the vertical (±35°) direction. These deformation features are present in both the melanorites and chromitite layers.

Most of the sulphides in the melanorite layers occur in a vertical network (Fig. 10), and most sulphide minerals are located at contacts between orthopyroxene crystals. Some of the orthopyroxene crystals have undergone deformation by dislocation creep, dissolution, or diffusion creep (Fig. 10). In the coarse-grained melanorite, sulphides were also found located in a vertical network along the contacts between orthopyroxene and deformed interstitial plagioclase crystals (Fig. 10). In contrast to the vertically elongate distribution of sulphides in the melanorites, the distribution of sulphides in the chromitite layer is in the form of isolated droplets (Fig. 6d) and they are not interconnected.

J-M Reef sample. The olivine melagabbronorite of the J-M Reef has undergone deformation during crystallization. This deformation is well displayed in the pyroxene

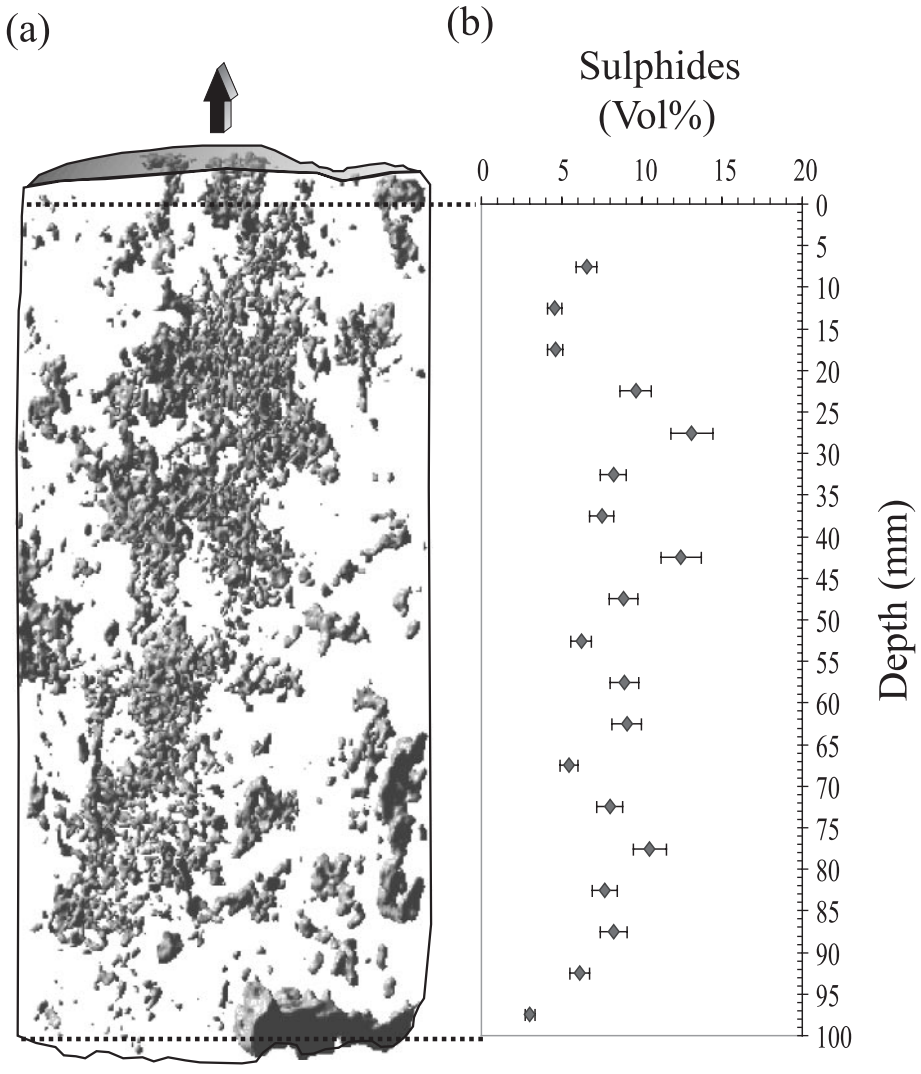

Fig. 9. Distribution of sulphide minerals in the J-M Reef sample based on results from CT scans. (a) Sulphide minerals are represented by grey shading. Paleovertical is represented by the black arrow. (b) Calculated content of sulphide minerals.

framework and the interstitial plagioclase. Some of the pyroxenes show indented contacts (Fig. 11). In all cases, the cleavage planes and exsolution lamellae are straight around contacts between pyroxene crystals. As in the case of the Merensky Reef sample, this indicates that deformation of the pyroxenes probably occurred by diffusion creep or dissolution. Some of the pyroxenes also exhibit undulose extinction and kinks (Fig. 11). Moreover, small clinopyroxene subgrains are well developed at the edges of crystals along contacts with other pyroxenes. These features indicate that the crystals have been affected by dislocation creep and recovery. Interstitial plagioclase shows evidence for deformation after the crystal mush was consolidated. Plagioclase exhibits spindle-shaped twins, bent twins, perpendicular twins and undulose extinctions. Generally, these twins are oriented at angles of about ±35° relative to the vertical. Furthermore, sulphide minerals are distributed along the crystal boundaries of deformed pyroxenes and rounded olivine and form vertically linked networks.

Deduction of the principal compressive stress direction during the formation of the cumulates

In both the Merensky Reef and J-M Reef samples, the deformation features of the crystals and the distribution of the sulphides are very similar (Figs 10 and 11). The principal compressive stress direction during formation of the cumulates can be inferred by considering the paleovertical orientation, orientation of deformation features and the location of the sulphide minerals described above. The pyroxenes exhibit undulose extinction, kinks,

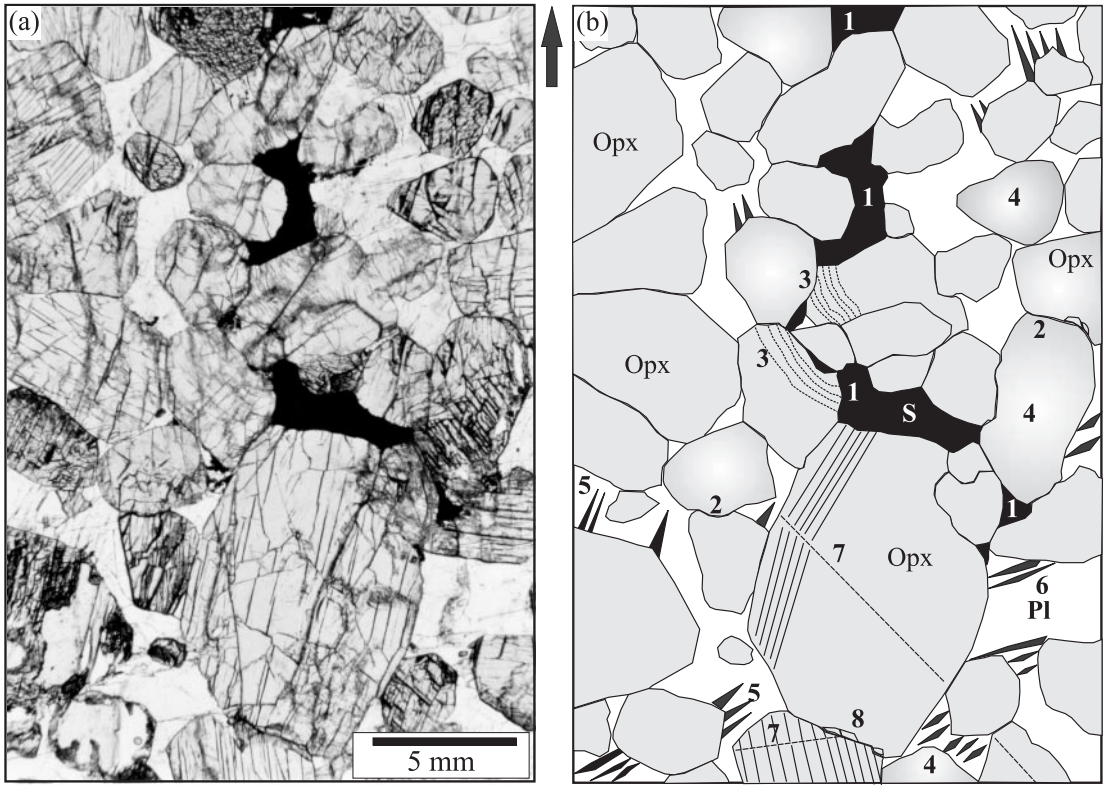

Fig. 10. Summary of microstructures observed in the Merensky Reef sample. Paleovertical is represented by the black arrow. (a) Photomicrograph of melanorite. (b) Sketch showing microstructures present in the photomicrograph (a): 1, sulphide minerals distributed along vertical segments and located between Opx contacts; 2, indented contact between Opx crystals; 3, bent Opx cleavage around indented contacts; 4, undulose extinctions in Px; 5, deformation twins with tapering edges in Pl nucleated on high-stress site; 6, spindle-shaped twins in Pl; 7, kink planes in Opx; 8, development of subgrains. Opx, orthopyroxene; Pl, plagioclase.

and subgrain development. Some cumulus pyroxene crystals have impinged on each other and indented contacts or subgrain developments are generally oriented along sub-horizontal pyroxene contacts, but not along vertical ones. The interstitial plagioclase is characterized by the presence of widespread deformation in the two samples. This intracrystalline deformation is demonstrated by the presence of spindle-shaped twins, bent twins, perpendicular twins, and undulose extinction. Deformation twins in plagioclase with tapering edges nucleated at high-stress sites at the edges of the crystals. In both samples, spindle-shaped twins, or bent twins, have a preferred shape orientation (Figs 10 and 11) close to the vertical ($\pm 35°$) direction. Late intercumulus minerals, such as biotite, do not show deformation features. Consequently, it seems that deformation occurred during the crystallization of pyroxenes and the interstitial plagioclase, but before the late minerals formed. Furthermore, sulphide minerals are, in many cases, located along pyroxene grain boundaries, and they form a vertical network along the faces of silicate crystals, mainly pyroxene or olivine. However, in the melanorite layer of the Merensky Reef, some of the sulphide minerals have crystallized at the contact between deformed plagioclase and pyroxene and these sulphide minerals form a vertical network, or elongate pockets of sulphide trapped and surrounded by plagioclase. In this case, it is possible that sulphide migration has been arrested as as result of the lack of permeability where extensive interstitial plagioclase crystallization had taken place.

As described by Barnes & Maier (2002), these high-temperature deformation features are consistent with a paleovertical maximum principal compressive stress (σ_1), and this is responsible for compaction during the formation of the cumulates. Thus, the distribution of the sulphide minerals is interpreted to indicate that they filled vertical dilatancies that formed between silicate mineral grain boundaries during compaction.

Connectivity of the sulphide melt

The distribution of melt in a solid matrix is controlled by the relative energies of crystal–crystal and crystal–melt interfaces. By considering that in a solid matrix (i.e. crystals), the surface energy is isotropic, the 3-D melt topology could be predicted by considering the

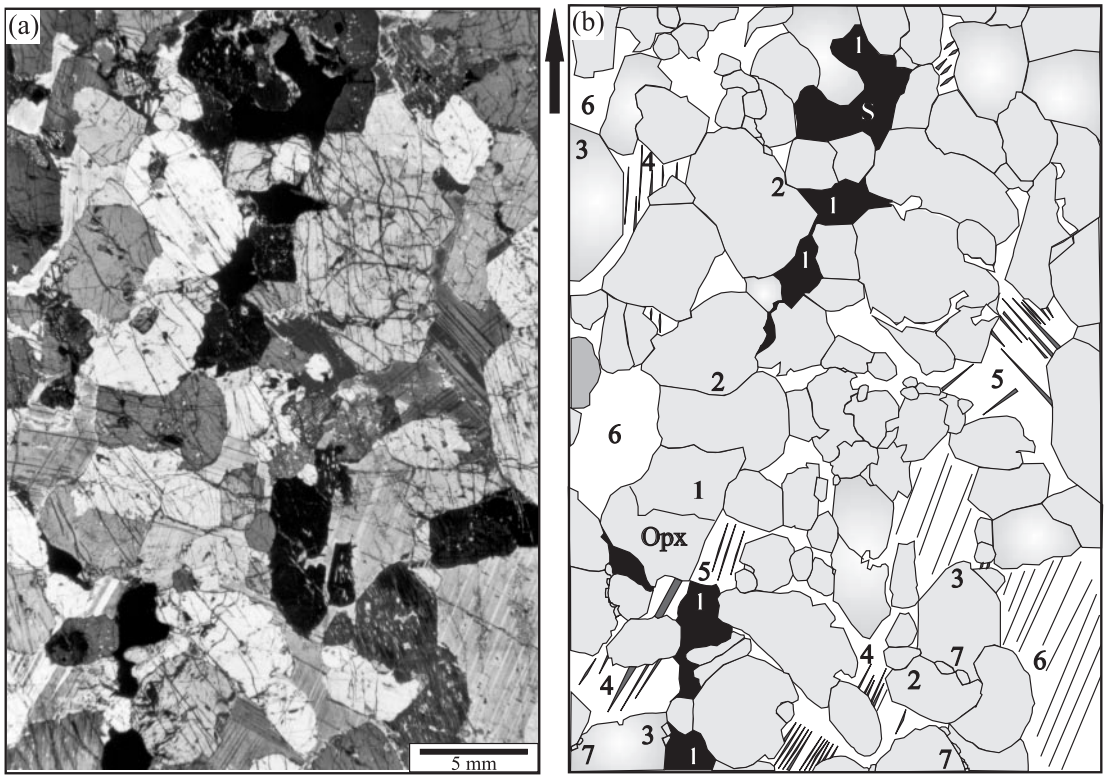

Fig. 11. Summary of microstructures observed in the J-M Reef sample. Paleovertical is represented by the black arrow. (a) Photomicrographs of gabbronorite. (b) Sketch showing microstructures present in the photomicrograph (a): 1, sulphide minerals distributed along vertical network and located between Opx contacts; 2, indented contacts between Opx crystals; 3, undulose extinction in Px; 4, deformation twins in Pl with tapering edges nucleated on high-stress site; 5, spindle-shaped twins in Pl; 6, undulose extinction in Pl; 7, development of subgrains in Opx. Opx, orthopyroxene, Px, pyroxene; Pl, plagioclase.

Table 3: Results of dihedral angle measurements in the Merensky Reef sample

Lithology	Minerals			Number of measurements	Median angle (°)	Angle (°)	
						Min.	Max.
Melanorite	Px	Px	S	89	51·5	18	123
Melanorite	Px	Pl	S	14	71·5	22	139
Melanorite		Total		103	53	18	139
Upper chromitite (UC)	Cr	Cr	S	86	95	37	144
Lower chromitite (LC)	Cr	Cr	S	55	103·5	35	139
Chromitite (UC and LC)	Cr	Cr	S	141	96·5	25	144

Px, pyroxene; Pl, plagioclase; Cr, chromite; S, sulphide minerals.

cross-sectional geometry of the solid–liquid interface (Watson & Brenan, 1987; Laporte & Provost, 2000; Rose & Brenan, 2001; Brenan & Rose, 2002; Holness *et al.*, 2005); in other words, by considering dihedral angles. At equilibrium, the dihedral angle (θ) at the contact between melt and two crystals is defined as

$$\theta = 2arcos(\gamma cc/2\gamma cm)$$

where γcc and γcm are the crystal–crystal and crystal–melt surface energies, respectively. Where $0 < \theta < 60°$, the melt is considered to wet crystal faces and is interconnected in three dimensions, even for a low melt fraction (Von Bargen & Waff, 1986). Where $\theta > 60°$, the melt is considered not to wet crystal faces and melt interconnectivity is not achieved at a low melt fraction (Von Bargen & Waff, 1986). Consequently, melt is

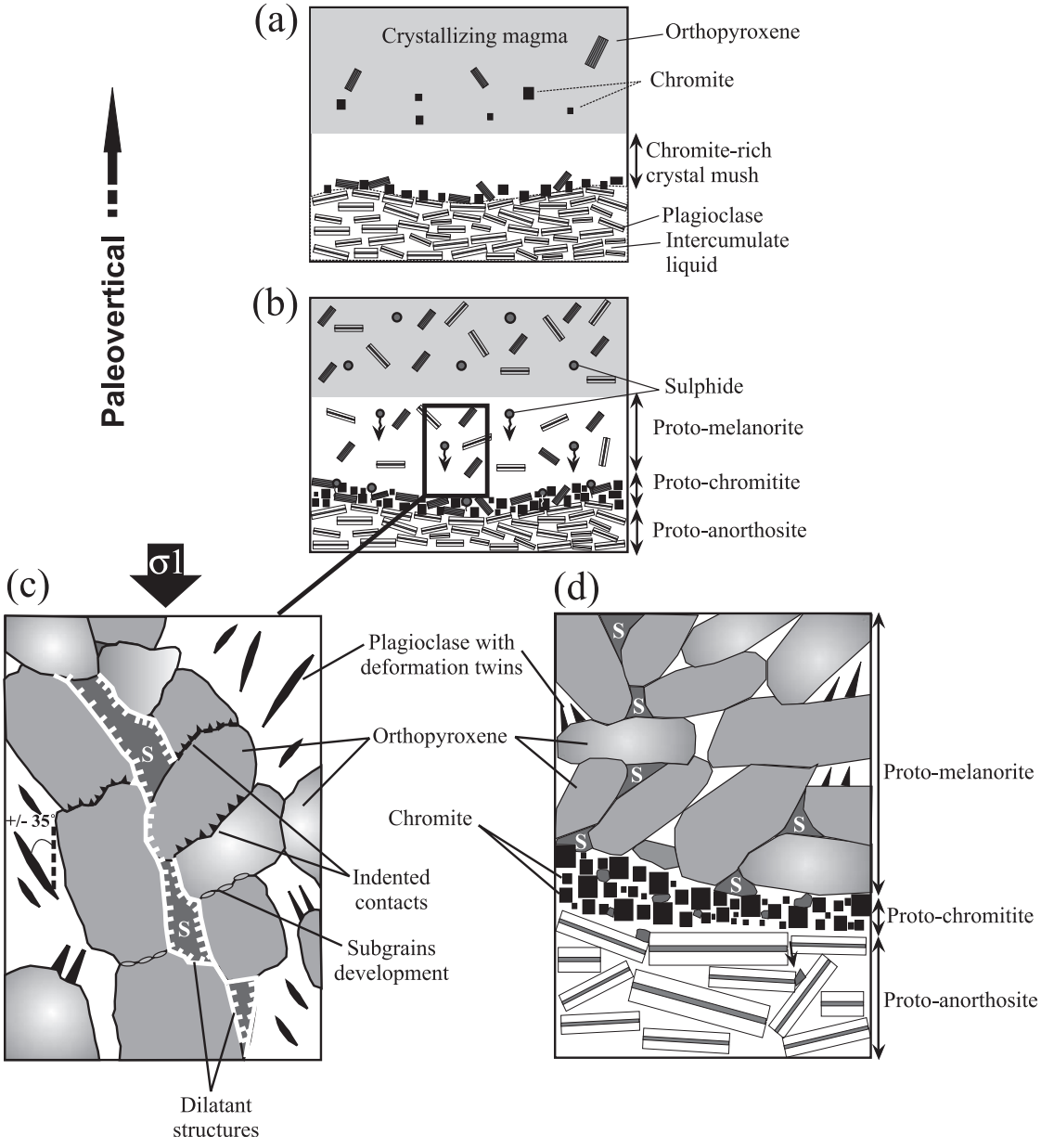

Fig. 12. Model of formation of the Merensky Reef. (a) Crystallization of chromite and orthopyroxene on cumulate pile to form chromite layer. (b) Immiscible sulphide liquid percolates into the cumulate pile. (c) High-temperature deformation (indented contact, deformation twins, undulose extinctions, subgrain development) in melanorite under a vertical principal compressive stress (σ_1) triggered by compaction of the cumulate pile. The downward percolation of sulphide liquid (S) through dilatant structures is improved by the compaction of the cumulate. (d) The vertical sulphide liquid network stops at the underlying chromitite layer because of the lack of interconnectivity of the sulphide liquid in this layer. Sulphides in the chromitite appear as small droplets. The chromitite seems to act as a filter, preventing extensive downward percolation of the sulphide liquid in the underlying anorthosite.

confined to isolated pockets at grain corners and the migration of melt is negligible. Thus measurements of the dihedral angles between sulphides and others minerals (silicates and/or oxides) in our samples can be used to characterize the sulphide melt topology and interconnectivity in these natural rocks. As the sulphides contained in the J-M Reef are partially altered, dihedral angles between sulphides and silicates are obscured by the alteration. Consequently, no measurements were made in the J-M Reef sample.

Dihedral angle measurements in the MR sample. To decide whether the sulphide liquid is interconnected or not in the melanorites and chromitite layers, the dihedral angles between sulphides and silicates and/or oxides

were measured from polished thin sections using an optical microscope. For each sample, a population of angles (>100 angles) were measured on the two-dimensional (2-D) thin sections, with an error on each measurement of a few degrees. Angles differ because of the anisotropy of interfacial energies, and can assume a range of values depending on the orientation of the crystal lattices. However, according to previous workers (Harker & Parker, 1945; Riegger & Van Vlack, 1960; Holness *et al.*, 2005; M. B. Holness, personal communication, 2005), the median angle of this 2-D angle population can be correlated (with a minor error of ~1°) with the true 3-D angle. Results obtained for the MR sample are summarized in Table 3.

In the melanorite, dihedral angles were measured at pyroxene–sulphide and plagioclase–sulphide junctions. Dihedral angles vary from 18 to 139°, but the median value of 103 measurements is 53°. In the chromitite layers, dihedral angles were measured at chromite–sulphide interfaces. In this case, dihedral angles vary from 25 to 144°, and the median value of 141 measurements is 95°. Thus, the sulphide liquid behaves differently in melanorite compared with chromitite layers. Dihedral angles between silicates and sulphide melt in the melanorite are <60°, which implies that the sulphide melt could have been interconnected and could have infiltrated the cumulate. In contrast, the dihedral angles in the chromitite layers, where sulphides occur as small droplets, are largely >60°, implying that sulphide melt connectivity is negligible. Consequently, sulphide melt percolation in chromitites is very limited.

DISCUSSION

The two samples examined in this study show considerable variation in lithology. The MR sample contains several distinct rock types (anorthosite, chromitite and melanorite) whereas the J-M Reef sample consists of a relatively homogeneous olivine melagabbronorite. Despite the difference in lithology between the MR and J-M Reef samples, the 3-D distribution of sulphide minerals and microstructures shows that both the reefs have several features in common.

Connectivity of the sulphide melt and the role of compaction

The dihedral angles measured in the MR sample, the distribution of the sulphides observed in thin section and the X-ray CT analysis showed that the sulphide minerals occur as an interconnected vertical network in the melanorite, which spreads out and is arrested in the chromitite layers. In the J-M Reef sample the distribution of sulphides observed in thin section and X-ray CT analysis shows that the sulphide minerals form a network interconnected vertically. Microstructural analysis indicates that both samples have undergone crystal deformation at high temperature (i.e. during crystallization of the cumulate minerals). The deformation was observed only in pyroxenes and interstitial plagioclase; late minerals such as biotite were not deformed. All deformation features are consistent with a principal compressive stress (σ_1) oriented sub-parallel to the paleovertical, and could have been induced by compaction of the crystal pile during formation of the cumulate.

In the Merensky Reef sample, the highest concentration of sulphide minerals was observed just above the two chromitite layers. We suggest that in the melanorites, sulphide melt accumulated at the top of the cumulate pile. During compaction of the pile, dilatancies formed between pyroxene and plagioclase crystals as a result of extension in the plane of the layer and the sulphide liquid migrated into these dilatant sites and downwards into the crystal pile.

Role of chromitite layers in the migration of sulphide melt

The most striking difference between the two samples is that the J-M Reef sample consists of one rock type, whereas the Merensky Reef sample consists of five layers and three rock types. In the Merensky Reef, the sulphides are concentrated in the troughs above the chromitite layers and then appear to form a cast of the chromitite layers. This observation could be explained by the difference in dihedral angles between sulphides and silicates and between sulphides and chromites. Because the sulphide melt could wet the silicates, it was able to percolate through the silicate pile. In contrast, the sulphide melt could not wet the chromites, thus the sulphide melt formed droplets against the chromite, ceased to be interconnected and could, therefore, no longer percolate through the cumulate pile.

Experimental studies by Rose & Brenan (2001) and Brenan & Rose (2002), at conditions close to FMQ (fayalite–magnetite–quartz buffer) and 1300°C, showed that wetting angles between olivine and sulphide liquid are higher than those between chromite and sulphide liquid. Thus, those workers suggested that sulphide melt will show a stronger interconnectivity in chromitite layers than in silicate (olivine) layers, contrary to our observations. We do not have an explanation as to why the experiments and the natural sample yield contradictory results.

Implications for the formation of the Merensky Reef

A number of workers (Campbell *et al.*, 1983; Naldrett *et al.*, 1986) have suggested that the Merensky Reef

formed from a new batch of magma injected into the magma chamber. At the base of the Merensky cycle, a layer of chromitite formed followed by melanorite (Fig. 12a). An immiscible sulphide liquid collected the PGE and then settled onto the crystal pile (Fig. 12b). On the basis of microstructural work at Impala Platinum Mines, Barnes & Maier (2002) modified this model and concluded that in 2-D space sulphides appear to have percolated downwards, and to have filled interstitial spaces in the crystal framework, thereby forming a sub-vertical network during compaction. Our results using different imaging techniques on the Merensky Reef at Rustenburg Platinum Mine and on the J-M Reef at Stillwater Mine suggest that this conclusion holds in three dimensions too (Fig. 12c). The sulphide networks in both melanorites of the MR sample terminate at their respective underlying chromitite (Fig. 12d). By considering a single chromitite layer and its overlying melanorite (supposed to have formed by one magmatic event), the sulphide mineral content increases from the top to the bottom in the melanorite (with a maximum value just above the chromitite) and the content of sulphides decreases from the top to the bottom in the chromitite layer. According to the dihedral angle measurements in this natural sample, sulphide migration in the chromitite was inhibited and, thus, extensive downward infiltration of a sulphide melt is unlikely (Fig. 12d). These interpretations are supported by the observation that in our sample the underlying anorthosite contains only minor sulphide mineralization. This point was made for the Merensky Reef in general by Viljoen *et al.* (1986) and Cawthorn (1999), who noted that the high abundance of sulphide at the level of the Merensky Reef strongly decreases in the footwall anorthosite. Cawthorn (1999) interpreted the decrease in the sulphide mineral content into the footwall of the Merensky Reef to be the result of the low permeability in the footwall. We suggest that another factor is the lack of interconnectivity of the sulphide melt in the chromitite layers. The sulphide liquid beaded in the chromitite layers thus impeding further downward migration. This resulted in high PGE contents of the chromitite layers.

CONCLUSIONS

X-ray computed tomography is a powerful technique allowing 3-D analysis and quantification of minerals in samples of tens of centimetres size. The analysis has highlighted the distribution of sulphide minerals in two samples from the Bushveld and Stillwater complexes. In the light of the results obtained for the MR and J-M Reef samples, it appears that downward migration of sulphide melt in a cumulate pile can be facilitated by compaction. Furthermore, connectivity of sulphide melt is high in melanorite and is negligible in chromitite layers of the MR sample. Thus, chromitite layers may play an important role in preventing further downward migration of sulphide melt. This could partially explain the enrichment of PGE in chromitite layers, and the decrease in the modal abundance of sulphide minerals in the footwall of the Merensky Reef.

ACKNOWLEDGEMENTS

Rustenburg Platinum Mine is thanked for allowing access to their properties and allowing sampling of the Merensky Reef. Stillwater Mining Company is thanked for hosting the '9th International Platinum Symposium' field trip and allowing sampling of the J-M Reef core. Paul Bedard (UQAC) is thanked for the suggestion that we use CT imaging to study the sulphide distribution. Edward Sawyer (UQAC) is thanked for proof reading early drafts of the manuscript. Jacques Labrie is thanked for assistance in using the INRS CT scanner facility. David Hirsch, Richard Kyle and Michael Zientek are thanked for their constructive reviews. This work was funded by a Discovery Grant from Natural Science and Engineering Research Council of Canada and the Canadian Research Chair in Magmatic Metallogeny.

SUPPLEMENTARY DATA

Supplementary data for this paper are available at *Journal of Petrology* online.

REFERENCES

Ballhaus, C. & Ryan, C. G. (1995). Platinum-group elements in the Merensky reef. I. PGE in solid solution in base metal sulfides and the down-temperature equilibration history of Merensky ores. *Contributions to Mineralogy and Petrology* **122**, 241–251.

Ballhaus, C. & Sylvester, P. (2000). Noble metal enrichment processes in the Merensky Reef, Bushveld Complex. *Journal of Petrology* **41**, 545–561.

Barnes, S.-J. & Maier, W. D. (2002). Platinum-group elements and microstructures of normal Merensky Reef from Impala Platinum Mines, Bushveld Complex. *Journal of Petrology* **43**, 103–128.

Barnes, S. J. & Naldrett, A. J. (1985). Geochemistry of the J-M (Howland) Reef of the Stillwater Complex, Minneapolis Adit Area. I. Sulfide chemistry and sulphide–olivine equilibrium. *Economic Geology* **80**, 627–645.

Boespflug, X., Long, B. F. N. & Occhietti, S. (1995). CAT-scan in marine stratigraphy: a quantitative approach. *Marine Geology* **122**, 281–301.

Boudreau, A. E. & McCallum, I. S. (1992). Infiltration metasomatism in layered intrusions—an example from the Stillwater Complex, Montana. *Journal of Volcanology and Geothermal Research* **52**, 171–183.

Brenan, J. M. & Rose, L. A. (2002). Experimental constraints on the wetting of chromite by sulfide liquid. *Canadian Mineralogist* **40**, 1113–1126.

Brochu, C. A. (2000). A digitally rendered endocast for *Tyrannosaurus rex*. *Journal of Vertebrate Paleontology* **20**, 1–6.

Campbell, I. H., Naldrett, A. J. & Barnes, S. J. (1983). A model for the origin of the platinum-rich sulfide horizons in the Bushveld and Stillwater complexes. *Journal of Petrology* **24**, 133–165.

Carlson, W. D. & Denison, C. (1992). Mechanisms of porphyroblast crystallization: results from high-resolution computed X-ray tomography. *Science* **257**, 1236–1239.

Cawthorn, R. G. (1999). Permeability of the footwall cumulates to the Merensky Reef, Bushveld Complex. *South African Journal of Geology* **102**, 293–302.

Delerue, J. F., Perrier, E., Timmermann, A. & Swennen, R. (2003). 3D soil image characterization applied to hydraulic properties computation. In: Mees, F., Swennen, R., Van Geet, M. & Jacobs, P. (eds) *Application of X-ray Computed Tomography in the Geosciences. Geological Society, London, Special Publications* **215**, 1–6.

Denison, C. & Carlson, W. D. (1997). Three-dimensional quantitative textural analysis of metamorphic rocks using high-resolution computed X-ray tomography. 2. Application to natural samples. *Journal of Metamorphic Geology* **15**, 45–57.

Denison, C., Carlson, W. D. & Ketcham, R. A. (1997). Three-dimensional quantitative textural analysis of metamorphic rocks using high-resolution computed X-ray tomography. 1. Methods and techniques. *Journal of Metamorphic Geology* **15**, 29–44.

Eales, H. V. & Cawthorn, R. G. (1996). The Bushveld Complex. In: Cawthorn, R. G. (ed.) *Layered Intrusions*. Amsterdam: Elsevier, pp. 181–230.

Flisch, A. & Becker, A. (2003). Industrial X-ray computed tomography studies of lake sediments drill cores. In: Mees, F., Swennen, R., Van Geet, M. & Jacobs, P. (eds) *Application of X-ray Computed Tomography in the Geosciences. Geological Society, London, Special Publications* **215**, 205–212.

Harker, D. & Parker, E. R. (1945). Grain shape and grain growth. *Transactions of the American Society of Metals* **34**, 156–195.

Harmer, R. E. & Armstrong, R. A. (2000). Duration of Bushveld Complex (*sensu lato*) magmatism: constraints from new SHRIMP zircon chronology. Workshop on the Bushveld Complex, Gethane Lodge, Burgersfort, abstracts and program.

Hiemstra, S. A. (1979). The role of collectors in the formation of the platinum deposits in the Bushveld Complex. *Canadian Mineralogist* **17**, 469–482.

Holness, M. B., Cheadle, M. J. & McKenzie, D. (2005). On the use of changes in dihedral angle to decode late-stage textural evolution in cumulates. *Journal of Petrology* **46**, 1565–1583.

Hounsfield, G. N. (1973). Computerized transverse axial scanning (tomography). 1. Description of system. *British Journal of Radiology* **46**, 1016–1022.

Johns, R. A., Steude, J. S., Castanier, L. M. & Roberts, P. V. (1993). Nondestructive measurements of fracture aperture in crystalline rock cores using X-ray computed tomography. *Journal of Geophysical Research* **98**(B2), 1889–1900.

Ketcham, R. A. & Carlson, W. D. (2001). Acquisition, optimization and interpretation of X-ray computed tomographic imagery: applications to the geosciences. *Computers & Geosciences* **27**, 381–400.

Ketcham, R. A. & Iturrino, G. J. (2005). Nondestructive high-resolution visualisation and measurement of anisotropic effective porosity in complex lithologies using high-resolution X-ray computed tomography. *Journal of Hydrology* **302**, 92–106.

Kinloch, E. D. (1982). Regional trends in the Platinum-Group mineralogy of the Critical Zone of the Bushveld Complex, South Africa. *Economic Geology* **77**, 1328–1347.

Kondo, M., Tsuchiyama, A., Hirai, H. & Koishikawa, A. (1997). High resolution X-ray computed tomographic (CT) images of chondrites and a chondrule. In: *21st Symposium on Antarctic Meteorites, Tokyo*, **10**, 437–447.

Kyle, J. R. & Ketcham, R. A. (2003). *In situ* distribution of gold in ores using high-resolution X-ray computed tomography. *Economic Geology* **98**, 1697–1701.

Kyle, J. R., Ketcham, R. A. & Mote, A. S. (2004). Contributions of high resolution X-ray computed tomography to ores studies. In: Muhling, J. (ed.) *Extended Abstracts, Predictive Mineral Discovery Under Cover*. Perth: University of Western Australia, pp. 387–390.

Laporte, D. & Provost, A. (2000). The grain-scale distribution of silicate, carbonate and metallosulfide partial melts: a review of theory and experiments. In: Bagdassarov, N., Laporte, D. & Thompson, A. B. (eds) *Physics and Chemistry of Partially Molten Rocks*. Dordrecht: Kluwer Academic, pp. 93–140.

Li, C., Ripley, E. M., Merino, E. & Maier, W. D. (2004). Replacement of base metal sulfides by actinolite, epidote, calcite, and magnetite in the UG2 and Merensky Reef of the Bushveld Complex, South Africa. *Economic Geology* **99**, 173–184.

McCallum, I. S., Raedeke, L. D. & Mathez, E. A. (1980). Investigations of the Stillwater Complex: Part I. Stratigraphy and structure of the Banded Zone. *American Journal of Science* **280-A**, 59–87.

Mees, F., Swennen, R., Van Geet, M. & Jacobs, P. (eds) (2003). *Applications of X-Ray Computed Tomography in the Geosciences. Geological Society, London, Special Publications* **215**.

Michaud, E., Desrosiers, G., Long, B., de Montety, L., Cremer, J.-F., Pelletier, E., Locat, J., Gilbert, F. & Stora, G. (2003). Use of axial tomography to follow temporal changes of benthic communities in an unstable sedimentary environment (Baie des Ha! Ha!, Saguenay Fjord). *Journal of Experimental Marine Biology and Ecology* **285–286**, 265–282.

Naldrett, A. J., Gasparrini, E. C., Barnes, S. J., Von Gruenewaldt, G. & Sharpe, M. R. (1986). The Upper Critical Zone of the Bushveld Complex and the origin of Merensky-type ores. *Economic Geology* **81**, 1105–1117.

Page, N. J. & Zientek, M. L. (1985). Geologic and structural setting of the Stillwater Complex. In: Czamanske, G. K. & Zientek, M. L. (eds) *The Stillwater Complex, Montana: Geology and Guide. Montana Bureau of Mines and Geology, Special Publications* **92**, 1–8.

Premo, W. R., Helz, R. T., Zientek, M. L. & Langston, R. B. (1990). U–Pb and Sm–Nd ages for the Stillwater Complex and its associated sills and dikes, Beartooth Mountains, Montana: identification of a parent magma? *Geology* **18**, 1065–1068.

Prichard, H. M., Barnes, S.-J., Maier, W. D. & Fisher, P. C. (2004). Variations in the nature of the platinum-group minerals in a cross-section through the Merensky Reef at Impala Platinum: implications for the mode of formation of the reef. *Canadian Mineralogist* **42**, 423–437.

Riegger, O. K. & Van Vlack, L. H. W. (1960). Dihedral angle measurement. *Transactions of the Mettalurgical Society of the AIME* **218**, 933–935.

Rose, L. A. & Brenan, J. M. (2001). Wetting properties of Fe–Ni–Co–Cu–O–S melts against olivine: implications for sulfide melt mobility. *Economic Geology* **96**, 145–157.

South African Committee for Stratigraphy (1980). Stratigraphy of Southern Africa. Part 1. Lithostratigraphy of South Africa, South West/Namibia, and the Republics of the Bophuthatswana, Transkei, and Venda. *Geological Survey of South Africa Handbook* **8**, 690.

Turner, A. R., Wolfgram, D. & Barnes, S. J. (1985). Geology of the Stillwater County sector of the J-M Reef, including the Minneapolis Adit. In: Czamanske, G. K. & Zientek, M. L. (eds) *The Stillwater Complex, Montana: Geology and Guide. Montana Bureau of Mines and Geology, Special Publications* **92**, 210–230.

Viljoen, M. J. & Hieber, R. (1986). The Rustenburg section of the Rustenburg Platinum Mines Limited, with reference to the Merensky Reef. In: Anhaeusser, C. R. & Maske, S. (eds) *Mineral*

Deposits of Southern Africa, II. Johannesburg: Geological Society of South Africa, pp. 1107–1034.

Viljoen, M. J., Theron, J., Underwood, B. M., Walters, J. & Peyerl, W. (1986). The Amandelbult section of Rustenburg Platinum Mines Limited, with reference to the Merensky Reef. In: Anhaeusser, C. R. & Maske, S. (eds) *Mineral Deposits of Southern Africa, II.* Johannesburg: Geological Society of South Africa, pp. 1041–1060.

Von Bargen, N. & Waff, H. S. (1986). Permeabilities, interfacial areas and curvatures of partially molten systems. Results of numerical computations of equilibrium microstructures. *Journal of Geophysical Research* **91**, 9261–9276.

Von Gruenewaldt, G. (1986). Platinum-group element–chromitite associations in the Bushveld Complex. *Economic Geology* **81**, 1067–1079.

Von Gruenewaldt, G. (1989). Contrasting platinum-group element concentration patterns in cumulates of the Bushveld Complex. *Mineralium Deposita* **24**, 219–229.

Watson, E. B. & Brenan, J. M. (1987). Fluids in the lithosphere, 1. Experimentally-determined wetting characteristics of CO_2–H_2O fluids and their implications for fluid transport, host-rock physical properties, and fluid inclusion formation. *Earth and Planetary Science Letters* **85**, 497–515.

Wellington, S. L. & Vinegar, H. J. (1987). X-ray computerized tomography. *Journal of Petroleum Technology* **39**, 885–898.

Wessel, P. & Smith, W. H. F. (1998). New, improved version of Generic Mapping Tools released. *EOS Transactions, American Geophysical Union* **79**, 579.

Willmore, C. C., Boudreau, A. E. & Kruger, F. J. (2000). The halogen geochemistry of the Bushveld Complex, Republic of South Africa: implications for chalcophile element distribution in the lower and critical zones. *Journal of Petrology* **41**, 1517–1539.

Zientek, M. L., Czamanske, G. K. & Irvine, T. N. (1985). Stratigraphy and nomenclature for the Stillwater Complex. In: Czamanske, G. K. & Zientek, M. L. (eds) *The Stillwater Complex, Montana: Geology and Guide. Montana Bureau of Mines and Geology, Special Publications* **92**, 21–32.

Zientek, M. L., Cooper, R. W., Corson, S. R. & Geraghty, E. P. (2002). Platinum-group element mineralization in the Stillwater Complex, Montana. In: Cabri, L. J. (ed.) *Geology, Geochemistry, Mineralogy and Mineral Benefication of Platinum Group Elements. Canadian Institute of Mining, Metallurgy and Petroleum, Special Volume* **54**, 459–481.